Purification of Human β and γ Actin from Budding Yeast

Brian K. Haarer (0000-0002-4018-222X)[1], Morgan L. Pimm (0000-0001-6370-1435)[1], Ebbing P. de Jong (0000-0002-0362-1772)[2], Jessica L. Henty-Ridilla (0000-0002-7203-8791)[1,3]✉, and David C. Amberg (0000-0002-4709-8848)[1]✉

[1]Department of Biochemistry & Molecular Biology, SUNY Upstate Medical University, Syracuse, NY, 13210
[2]Mass Spectrometry Core Facility, SUNY Upstate Medical University, Syracuse, NY, 13210
[3]Department of Neuroscience & Physiology, SUNY Upstate Medical University, Syracuse, NY, 13210

Biochemical studies of human actin and its binding partners rely heavily on abundant and easily purified α-actin from skeletal muscle. Therefore, muscle actin has been used to evaluate and determine the activities of most actin regulatory proteins and there is an underlying concern that these proteins perform differently with actin present in non-muscle cells. To provide easily accessible and relatively abundant sources of human β- or γ-actin (i.e., cytoplasmic actins), we developed *Saccharomyces cerevisiae* strains that express each as their sole source of actin. Both β- or γ-actin purified in this system polymerize and interact with various binding partners, including profilin, cofilin, mDia1 (formin), fascin, and thymosin-β4 (Tβ4). Notably, Tβ4 binds to β- or γ-actin with higher affinity than to muscle α-actin, emphasizing the value of testing actin ligands with specific actin isoforms. These reagents will make specific isoforms of actin more accessible for future studies of actin regulation.

cytoplasmic actin | non-muscle actin | β-actin | γ-actin
Correspondence: *ambergd@upstate.edu & ridillaj@upstate.edu*

Introduction

The actin cytoskeleton is an essential, highly conserved, and abundant component of cells. Simple eukaryotes tend to express a single actin isoform, while humans display tissue and cell specific expression patterns. Although closely related, actin isoforms can subtly differ in biochemical properties related to polymer formation, nucleotide hydrolysis and exchange, and interactions with one or more essential regulatory proteins (Allen et al., 1996; Moradi et al., 2017; Namba et al., 1992; Perrin and Ervasti, 2010). Humans express six actin isoforms: α1, α2, α-cardiac, and γ2 occur predominantly in skeletal, cardiac, and smooth muscle cells, whereas two isoforms β and γ1 (referred to as γ throughout) are found predominantly in non-muscle cells and are considered cytoplasmic isoforms actin. Human β- and γ-actin differ by only four amino acids located within their first ten amino acids (Figure 1A). Common sources of actin for use in biochemical studies are purified as a mixture of multiple isoforms from animal muscle, with only minor amounts of cytoplasmic actin. Further, commercial sources of cytoplasmic actin are less common and are often provided as a mixture of isoforms. Thus, it has been challenging to discern the biochemical properties of purified non-muscle actin isoforms.

Producing recombinant human actin outside of eukaryotic cells is difficult due to the complex network of chaperones needed to properly fold actin, however several systems have been developed (Geissler et al., 1998; Grantham, 2020; Millan-Zambrano and Chavez, 2014; Valpuesta et al., 2002). The pCold system permits the bacterial synthesis of recombinant tagged β-actin (Tamura et al., 2011). Actin isoforms expressed and purified from popular eukaryotic systems produce relatively large quantities of biochemically active actin (Bergeron et al., 2010; Bookwalter and Trybus, 2006; Ohki et al., 2009; Rutkevich et al., 2006; Yamashiro et al., 2014). While these and related purification methods have been adopted for various studies of normal and mutant versions of actin, preparations are often contaminated with low amounts (5-15%) of host actin (Hundt et al., 2014; Muller et al., 2013; Muller et al., 2012; von der Ecken et al., 2016). Other systems use a combination of affinity tags and a direct fusion to the actin monomer binding protein thymosin-β4 (Tβ4) to prevent the spurious polymerization or aggregation of recombinant actin and to facilitate isoform specific purification (Hatano et al., 2018; Hatano et al., 2020; Kijima et al., 2016; Noguchi et al., 2007). With additional modifications this approach permits the isolation of actin isoforms and of specific post translational states: N-acetylation, N-arginylation, and methylation of a conserved histidine residue (Hatano et al., 2018; Hatano et al., 2020). While each system requires post-purification processing, they provide a source of non-muscle, normal or mutant (including non-polymerizable), actin isoforms.

We have taken a different approach to generate pure human β- or γ-actin, engineering the yeast *Saccharomyces cerevisiae* to produce either isoform as their only source of actin. This technique was first pioneered to purify chicken β-actin from yeast, relying on hydroxylapatite chromatography to separate host and recombinant actin (Karlsson, 1988). A follow-up study showed that yeast could survive, albeit not well, with this as their sole actin source, although β-actin was not purified from these yeast strains (Karlsson et al., 1991). We have taken codon-optimized genes for human β- and γ-actin and expressed them in yeast lacking the resident actin gene, *ACT1*. The resulting strains grow considerably slower than wild type yeast yet can provide significant yields of homogeneous β- or γ-actin. While actin purified by this approach may not undergo standard N-terminal processing, each actin isoform polymerizes and interacts with several actin-binding proteins including cofilin, profilin, Tβ4,

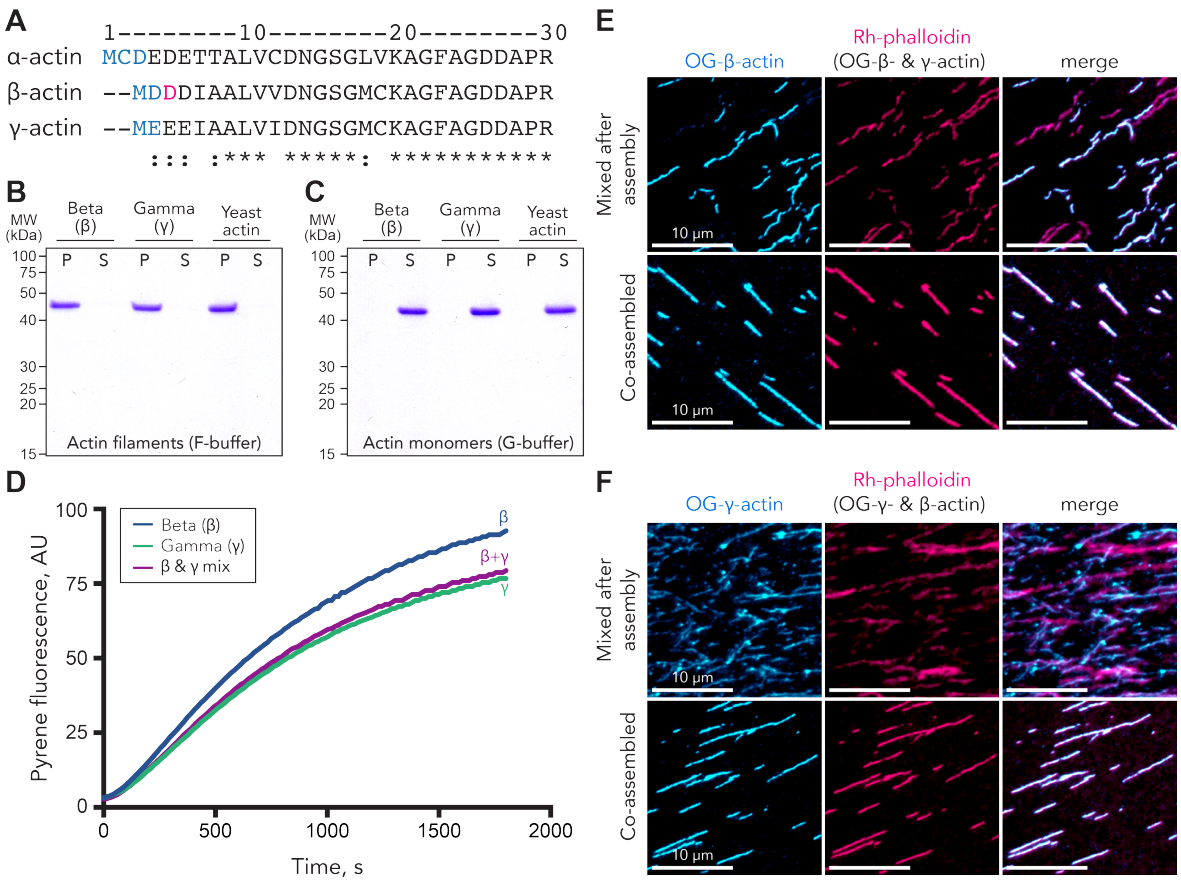

Figure 1. Yeast-made human β- and γ-actin form filaments and co-polymers. **(A)** Sequence alignment of the amino-terminal regions of human α1-, β-, and γ1-actin made with Clustal Omega (https://www.ebi.ac.uk/Tools/msa/clustalo/). Relevant modified residues are labeled as follows: acetylation (blue) and arginylation (pink). **(B-C)** Coomassie-stained SDS-PAGE gel from actin filament pelleting assays using 2.5 μM β-actin, γ-actin, or yeast actin performed in (B) actin filament (F-buffer) or (C) actin monomer buffer (G-buffer). **(D)** Polymerization of 2 μM (5% isoform specific pyrene label) β- (blue) or γ-actin (green) in a bulk fluorescence assay. The mixed reaction (magenta) contains 1 μM β- and 1 μM γ-actin (2 μM total). **(E)** Oregon Green (OG)-labeled β-actin and unlabeled γ-actin were polymerized separately, stabilized with rhodamine (Rh)-phalloidin, and then mixed (top) or co-polymerized (mixed, then polymerized) and stained with rhodamine-phalloidin (bottom). **(F)** Similar reactions as in (E) with OG-labeled γ-actin and unlabeled β-actin stained with Rh-phalloidin. Scale bars, 10 μm.

the formin mDia1, and fascin. Thus, these engineered strains provide consistent sources of pure β- or γ-actin for biochemical studies where conventional α-actin sources may be unsuitable.

Methods

Reagents and Supplies.

Unless otherwise specified, chemicals and supplies were purchased from Fisher Scientific (Pittsburgh, PA). DNaseI for affinity columns was purchased from Worthington Biochemical (Lakewood, NJ). Cloning reagents were obtained as follows: Restriction enzymes and DNA ligase (New England Biolabs; Ipswich, MA); Primestar HS DNA polymerase (Takara Bio USA; San Jose, CA); Oligonucleotides (Eurofins Genomics; Louisville, KY).

Plasmid and strain construction.

Human β-actin (ACTB; NCBI Gene ID: 60) and α1-actin (ACTA1; NCBI Gene ID: 58) genes flanked by *Bam*HI and *Hin*dIII sites were codon-optimized for expression in budding yeast (Figures S1A and S1B) (GenScript; Piscataway, NJ). Codon-optimized γ1-actin (ACTG1; NCBI Gene ID: 71) was generated from the optimized ACTB plasmid using a mutagenic primer to alter the appropriate N-terminal codons. Plasmids used for human actin production were made by inserting the codon-optimized genes downstream of the constitutive *TDH3* promoter, which was PCR amplified as an *Eco*RI-*Bam*HI fragment from yeast genomic DNA and inserted in the high copy number (2μ-based) yeast plasmid YEp351. The yeast strain expressing only β-actin (BHY845) is a haploid segregant of an *ACT1/act1*Δ heterozygous diploid that carried the β1-actin expression plasmid. The yeast strain that expresses only γ1-actin (BHY848) was generated by introducing the γ1-actin expression plasmid into a haploid *act1*Δ strain carrying the yeast *ACT1* gene on a *URA3*-based plasmid, then screening for growth on 5-fluoroorotic acid (FOA) media to select for cells that lost the *ACT1 (URA3)* plasmid but remained viable due to the presence of the γ1-actin-expressing plasmid. We were unable to recover yeast strains expressing only human α1-actin.

Human cofilin (CFL1; NCBI Gene ID: 1072) was cloned by PCR from cDNA prepared from HEK293 cells and inserted into expression plasmid pGST-parallel (Sheffield et al., 1999). The coding sequence for human profilin-1 (PFN1;

NCBI Gene ID: 5216) was cloned by PCR from cDNA and inserted into plasmid pKK223-3 (Pharmacia Biotech). All primer sequences used for plasmid construction are available in Table 1.

Protein purification.

All actin (yeast or human β- and γ-isoforms) were prepared as described for yeast actin previously (Aggeli et al., 2014), with the following modifications: yeast were grown in 1 L batches in YPD medium (1% yeast extract, 2% bactopeptone, 2-4% glucose), harvested by centrifugation at 8000 × *g* for 7 min, then washed in 25 mL 10 mM Tris (pH 7.5), 0.2 mM $CaCl_2$, and transferred to 50 mL conical tubes. Following centrifugation at 4000 × *g* for 10 min, pellets were frozen and stored at -80 °C. Pellets were suspended in 15-20 mL G-buffer (10 mM Tris (pH 7.5), 0.2 mM $CaCl_2$, 0.5 mM ATP, 0.2 mM DTT) plus protease inhibitors (0.1 mM PMSF and 1:500 Cocktail IV (Calbiochem; San Diego, CA) and lysed by two passes through a French press at ~1000 psi. Lysates were loaded on 3 mL DNaseI-Sepharose columns and washed sequentially with five bed volumes of G-buffer containing (1) 10% formamide, (2) 0.2 M NH_4Cl, and (3) no additive. Each actin isoform was eluted with G-buffer containing 50% formamide. Eluates were immediately diluted into 1-2 mL of G-buffer. Diluted eluates were loaded into Slide-A-Lyzers (10k MWCO; ThermoFisher Scientific; Waltham, MA) and dialyzed overnight against 2 L G-buffer. Contaminating proteins and polymerization incompetent actin were removed with the addition of KCl to 0.6 M and two or more de/polymerization cycles.

Human cofilin was expressed as a GST fusion in *E. coli* Rosetta cells. Following overnight induction with 0.4 mM IPTG at 30 °C, cells were suspended in TBS (50 mM Tris (pH 7.5), 100 mM NaCl) and lysed by two passes through a French press at 1000 psi. The lysate was clarified by centrifugation at ~17,000 × *g* for 30 min, then mixed with 2 mL glutathione agarose affinity resin by end-over-end rotation for 1 h at 4 °C. The resin was loaded into a column and washed twice with 10 mL TBS. GST-cofilin was eluted in three fractions of 2 mL with 3 mg/mL reduced glutathione resuspended in 50 mM Tris (pH 8) and 1 mM DTT. GST-cofilin was cleaved with TEV protease, leaving a residual glycine-alanine dipeptide at the N-terminus and dialyzed against 10 mM Tris (pH 7.5), 100 mM NaCl, 0.5 mM DTT at 4 °C in a 7000 MWCO Slide-A-Lyzer overnight. Cleaved GST and GST-TEV was removed by incubating dialysate with 1 mL glutathione agarose for 2 h at 4 °C and centrifugation at 15,000 × *g* for 10 min. The cleaved cofilin eluate was concentrated to 1 mL, clarified by centrifugation at 15,000 × *g* for 10 min, and loaded on a Superdex 75 gel filtration column (1.6 × 50 cm) pre-equilibrated with 20 mM Tris (pH 7.5), 100 mM NaCl, and 0.2 mM DTT. Peak fractions were combined, buffer exchanged into the same buffer without NaCl, and concentrated to 80 µM using Vivaspin 5000 centrifugal concentrators (Sartorius; Göttingen, Germany). Yeast cofilin was prepared as described previously (Aggeli et al., 2014; Clark and Amberg, 2007).

Untagged profilin-1 used in pelleting assays was expressed in *E. coli* Rosetta cells, induced with IPTG for 4 h at 30 °C. Cultures were lysed by French press and affinity purified on poly-*L*-proline beads (Haarer et al., 1990). Profilin-1 was dialyzed into 2 mM Tris (pH 7.5), 0.1 mM $CaCl_2$, and 0.2 mM DTT. Rabbit muscle actin ((RMA); α-actin), mDia1(FH1-C) (amino acids 571-1255), GFP-thymosin-β4, profilin-1, and fascin used in TIRF or anisotropy assays were purified as described (Jansen et al., 2011; Liu et al., 2022; Pimm et al., 2022). Actin isoforms were fluorescently labeled with pyrene-iodoacetamide or Oregon Green 488-iodoacetamide as described (Aggeli et al., 2014). Proteins were aliquoted, flash-frozen in liquid nitrogen, and stored at -80 °C.

Mass spectrometry analysis.

Actin bands were excised from Coomassie-stained 10% polyacrylamide gels and subjected to in-gel trypsin digestion (Shevchenko et al., 2006). Resulting peptides were extracted in 50% and 80% acetonitrile (ACN) and dried in a vacuum concentrator. Peptides were redissolved in 60 µL of 0.1% trifluoroacetic acid (TFA), and further purified using 2-core MCX stage tips activated with ACN, followed by 3% ACN with 0.1% TFA (Rappsilber et al., 2003). Samples were applied to tips, then washed twice with 3% ACN plus 0.1% TFA, and once with 65% ACN plus 0.1% TFA. Peptides were eluted in 75 µL of 65% ACN with 5% NH_4OH, and dried. Prior to injection, dried samples were redissolved in 30 µL of 2% ACN with 0.5% formic acid.

LC-MS analysis was performed using a Waters nanoAcquity LC and autosampler coupled to an Orbitrap XL hybrid ion trap Orbitrap mass spectrometer. Two µL of sample was injected onto a reversed phase nano LC column (PicoFrit [New Objective, Littleton, MA], 75 µm I.D. with 15 µm tip packed with 10 cm of BioBasic C18, 5 µm particles). A linear LC gradient from 2 to 35% ACN with constant 0.1% formic acid over 45 min was used, followed by a short ramp to 90% ACN and re-equilibration to 2% ACN for a total run time of 60 min. The LTQ-Orbitrap was operated in a top-five data-dependent mode using survey scans at 30,000 resolution from 375-1800 m/z. Tandem MS scans were acquired in the ion trap with an isolation width of 2 m/z and fragmentation mode was CID with 35% normalized collision energy for 0.1 ms. The automatic gain control settings were $3{\times}10^5$ ions in the ion trap, and $1{\times}10^6$ in the Orbitrap. Dynamic exclusion was used with a duration of 15 s and a repeat count of 1.

Tandem mass spectra were searched against a yeast database, human β- and γ-actin, and common contaminant proteins using the Sequest HT node in Proteome Discoverer 1.4. Search parameters included fixed modification of carbamidomethylation on cysteine, and partial trypsin specificity with two missed cleavages allowed. Variable modifications included methionine oxidation and protein N-terminal acetylation. To detect alternatively processed forms of actin, modified human actin sequences were added to the databases, including the deletion of N-terminal methionine and replacement of N-terminal methionine with arginine. Search results

were filtered to Percolator q-values < 0.01 and peptide confidence filter set for "high".

F-actin sedimentation assays.

Polymerization of 2-2.5 μM β- or γ-actin was induced with the addition of concentrated (20×) F-buffer (final 1× concentration: 10 mM Tris (pH 7.5), 25 mM KCl, 4 mM $MgCl_2$, 1 mM EGTA, 0.5 mM ATP). An equivalent amount of G-buffer was used for controls (unpolymerized actin). Samples were incubated for 30-40 min at room temperature, then subjected to centrifugation at 200,000 × *g* for 30 min at 20 °C. Supernatants were removed and pellets and supernatant samples were brought to equal volumes in protein loading buffer. Protein samples were incubated at 95 °C for 3 min, equal volumes were loaded on 4-15% SDS-polyacrylamide gels (BioRad, Hercules, CA), and stained with Coomassie. For cofilin-actin binding assays (Figures 3A and 3B), 4 μM cofilin was combined with 2.5 μM actin in G-buffer or F-buffer, and then incubated for 20 min at room temperature prior to centrifugation as above. For profilin binding assays, indicated concentrations of profilin (Figures 3D and 3E) was mixed with 2 μM actin monomers in G-buffer and then incubated for 30 min at room temperature. Actin polymerization was then induced with F-buffer for an additional 20 min prior to centrifugation as above.

Fluorescence-based actin polymerization assays.

Fluorescence readings of polymerizing 2 μM β- or γ-actin monomers (5% 1-pyrene-iodoacetamide labeled β- or γ-actin) in F-buffer were taken at 15 s intervals for 20 min in a spectrofluorometer set to 365 nm excitation and 385 nm emission (FluoroMax-4 spectrofluorometer; Horiba Scientific, Kyoto, Japan). Actin polymerization end-point fluorescence measurements for various concentrations of actin monomers (5% pyrene labeled) were taken after 10 min room temperature incubation in 150 μL of 1× F-buffer.

Actin isoform co-polymerization reactions were assessed by epifluorescence microscopy (Zeiss Imager.Z1, Oberkochen, Germany). 2 μM OG-labeled β- or γ-actin were polymerized in F-buffer, either individually or in various 1:1 mixtures of labeled:unlabeled actin, then bound to 1.1 μM rhodamine-phalloidin to simultaneously label filaments and block filament depolymerization. For samples that were polymerized and stabilized prior to mixing, equal amounts of phalloidin-stabilized actin were mixed seconds before viewing. Samples were viewed individually or as mixtures bound to phalloidin prior to mixing. Samples were flowed into homemade slide chambers prepared by laying a cover glass onto a slide with two intervening strips of double-sided tape, then visualized with DsRed and FITC filter sets. Views of were obtained near fluid/air boundaries.

Total Internal Reflection Fluorescence (TIRF) microscopy assays.

TIRF imaging chambers were prepared and visualized as described in detail (Henty-Ridilla, 2022) with the following modifications: reactions examining polymerization rates alone or with formin utilized unlabeled β- or γ-actin mixed with 10% Oregon Green or Alexa-488 labeled α-actin from rabbit muscle (RMA; <5-6% total label per reaction) and <0.1% biotin-labeled RMA. Reactions examining association with fascin used unlabeled actin (β-, γ-, or RMA) at 1 μM with <0.1% biotin-labeled RMA and without or with 1 μM fascin and were visualized by the addition of Alexa-488 phalloidin (130 nM) to the polymerization mix. Time lapse images were recorded at 5 s intervals (50 ms exposure) on a DMi8 inverted TIRF microscope (Leica Microsystems; Wetzlar, Germany) equipped with 120-150 mW solid-state lasers, a 100× Plan Apo 1.47 N.A. oil-immersion TIRF objective, and an iXon Life 897 EMCCD camera (Andor; Belfast, Northern Ireland). Polymerization rates (subunits s^{-1} μM^{-1}) were determined by measuring filament lengths from at least 5 frames, with conversion factor of 370 subunits/μm. Total filament or filament bundle length of Alexa-488 phalloidin-labeled actin was calculated using the FIJI Ridge Detection plugin (Schindelin et al., 2012; Steger, 1998; Wagner et al., 2017). Ridge Detection threshold settings minimized background signals but permitted the detection of faint filaments and robust bundles without saturation and were applied identically to all images analyzed (line width 0.2, high contrast 250, low contrast 0, sigma 0.56, lower threshold 0.00, upper threshold 17, minimum line length 1.00). Skewness was measured in FIJI on TIRF images with thresholds similar to the Ridge Detection analysis, above (Higaki et al., 2010; Khurana et al., 2010).

Fluorescence polarization assays.

Fluorescence polarization determination of GFP-thymosin-β4 (Tβ4) binding to actins (Liu et al., 2022) was carried out in 1× PBS (pH 8.0) supplemented with 150 mM NaCl. 10 nM β- or γ-actin were mixed with concentrations (0.1 pM to 10 μM) of GFP-Tβ4 and incubated at room temperature for 15 min. Fluorescence polarization was measured in a plate reader equipped with monochromator, with excitation at 440 nm and emission intensity detection at 510 nm (bandwidth set to 20 nm) (Tecan; Männnedorf, Switzerland). Three technical replicates were carried out on the same plate. Data were analyzed and binding constants determined as described previously (Liu et al., 2022).

Results

We expressed codon-optimized human cytoplasmic β- or γ-actin in *Saccharomyces cerevisiae* strains lacking the sole yeast actin gene (*ACT1*). The strain expressing human β-actin grew slowly (Figure S2) and displayed heterogeneous morphology, similar to yeast expressing chicken β-actin (Karlsson et al., 1991). The strain expressing γ-actin grew even more slowly, yet either strain could be maintained without additional selection with each plasmid-borne actin gene. To confirm the identify and assess the posttranslational state of either isoform, each recombinant actin was purified by conventional DNaseI affinity chromatography and subjected to mass spectrometry (MS). This analysis showed 82.4% (β-actin) and 89.9% (γ-actin) coverage of the predicted peptide

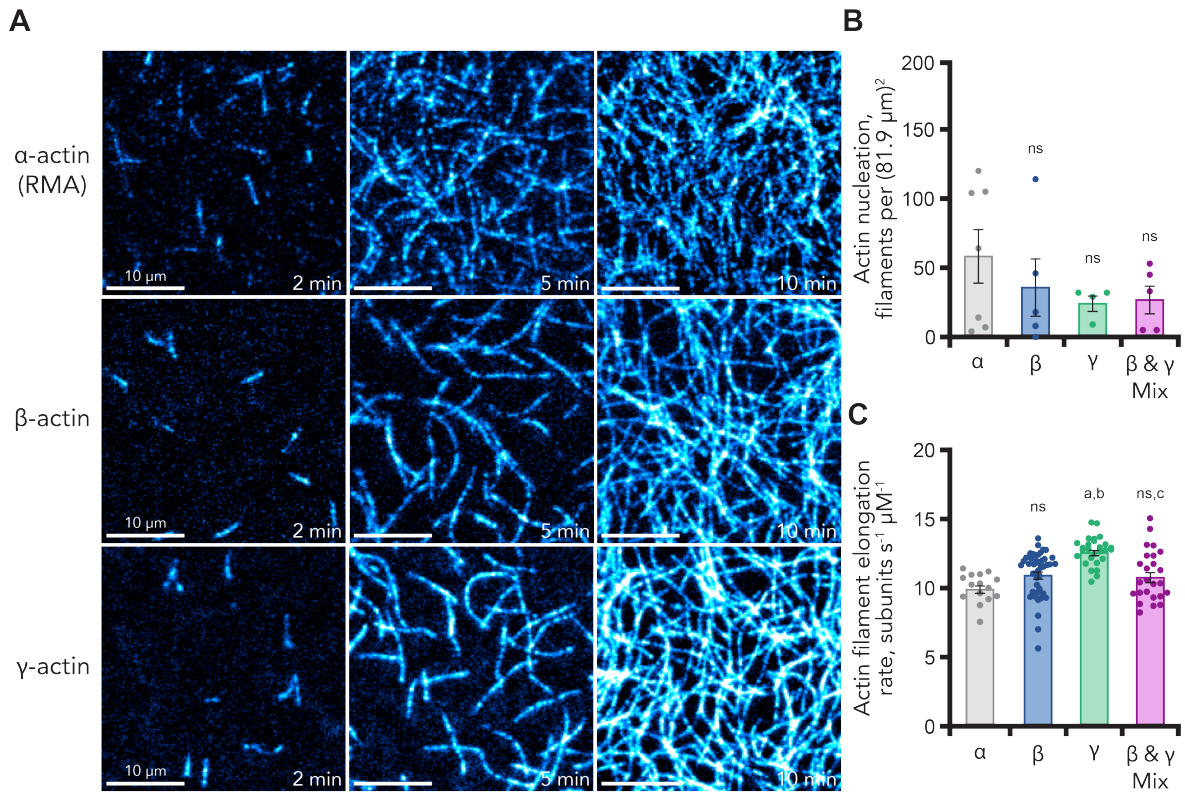

Figure 2. Actin isoforms display similar phases of actin assembly. (A) Images from time-lapse TIRF microscopy reactions containing 1 μM of each actin isoform (10% Alexa-488 labeled α-actin (RMA)). Scale bars, 10 μm. See also Movie 1. **(B)** Actin nucleation per (81.9 μm)^2 field of view (n = 3-6; represented as dots) counted from reactions as in (A) 100 s after the initiation of filament polymerization. **(C)** Actin filament elongation rate from reactions as in (A). Dots represent individual measurements. Error bars indicate SEM. a, significantly different ($p<0.05$) than α-actin (RMA) control; b, significantly different than β-actin; c, significantly different than γ-actin. Significant differences were determined by one-way ANOVA with Tukey post-hoc analysis.

profiles for each actin isoform. Notably, differences in MS profiles were detected in processing of the N-terminal peptide, which is the only predicted peptide that differs between β- and γ-actin (Figure 1A). Only N-terminally acetylated γ-actin (at Met1) was detected in this analysis. In contrast, no acetylated or intact N-terminal peptide was detected for β-actin. Instead, MS detected peptides lacking the first two (MD) or three (MDD) amino acids. We also detected a peptide that may correspond to arginylation of β-actin at Asp3 (RDDIAALVVDNGSGMCK). For comparison, MS analysis of yeast actin showed 85.3% coverage, with the majority of its N-terminal peptide matches indicating acetylation on Met1. Notably, peptides lacking the first one (M) or two (MD) amino acids were also detected in yeast actin preparations, suggesting the final state of each recombinant actin is influenced by host processing enzymes.

We assessed the ability of the β- and γ-actin isoforms to polymerize into filaments with conventional pelleting assays (Figure 1B). Polymerization of β-, γ-, or yeast actin (control) was indistinguishable, pelleting under conditions that promote actin filament assembly, and remaining in the supernatant in control reactions performed in low ionic strength G-buffer (Figure 1C). To further assess the polymerization kinetics of pure β- and γ-actin, we pyrene-labeled each isoform to perform fluorescence-based actin assembly assays. Each individual isoform polymerized as expected (Figure 1D), with critical concentrations between 0.15 and 0.25 μM (Belmont et al., 1999; Wang et al., 1989; Wen et al., 2002). To address whether β- and γ-actin could co-polymerize, we performed assays combining at equal stoichiometry (Figure 1D). Indeed, reactions containing both isoforms polymerized consistent with filament co-polymerization. To further confirm that β- and γ-actin filament co-polymerization occurs, we performed epifluorescence microscopy to visualize actin filaments polymerized before or after mixing unlabeled and Oregon Green (OG)-labeled β- or γ-actin bound to rhodamine(Rh)-phalloidin (Figure 1E-F). Rh-phalloidin stabilization of actin polymerized before mixing resulted in a mixed population of filaments including: Rh-phalloidin-decorated unlabeled actin only visible in the Rh-phalloidin channel; and, a few OG-labeled filaments co-labeled with Rh-phalloidin present in both channels (Figure 1E-F, top panels). In contrast, Rh-phalloidin stabilization of either actin co-polymerized produced filaments uniformly labeled actin filaments in both wavelengths, consistent with co-polymerization. Notably, filament co-labeling occurred regardless of which actin is OG-labeled, consistent with co-polymerization of β- and γ-actin (Figure 1E-F, bottom panels). To further assess the actin assembly properties of β- and γ-actin, we used total internal reflection fluorescence (TIRF) microscopy to directly observe single actin filament polymerization (Figure 2A). In these experiments unlabeled 1 μM β-actin, γ-actin or control α-actin purified from rabbit muscle (RMA) was visualized with 10% fluorescently labeled RMA

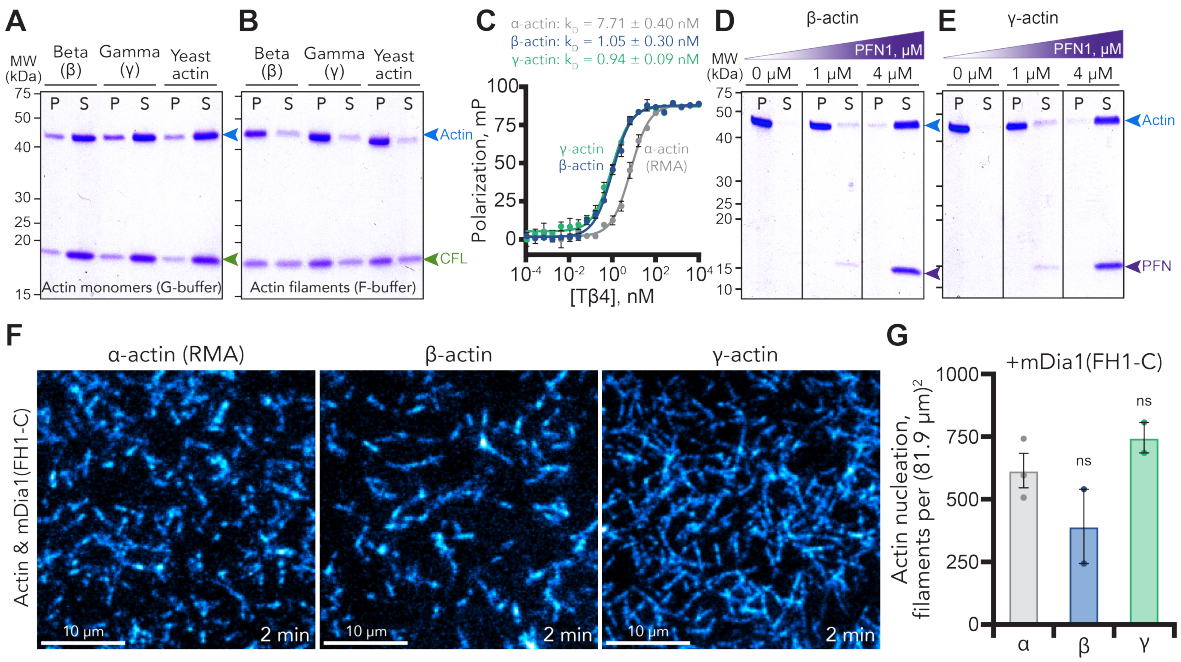

Figure 3. Effects of diverse actin regulation proteins on β- or γ-actin. (A-B) Coomassie-stained SDS-PAGE gel from actin filament pelleting assays with 4 μM cofilin-1 (CFL1; green arrow) and 2.5 μM β-actin, γ-actin, or yeast actin (blue arrow) performed in (A) actin monomer buffer (G-buffer) or (B) actin filament (F-buffer). **(C)**Fluorescence polarization of varying concentrations of GFP-Tβ4 mixed with 10 nM unlabeled β-(blue), γ-(green) or α-actin (RMA; grey). Curves shown are average fits from n = 3 separate experiments. Error bars indicate SEM. **(D-E)** Coomassie-stained SDS-PAGE gel from actin filament pelleting assays with varying concentrations of profilin-1 (PFN1; purple arrow) and 2 μM (D) β-actin or (E) γ-actin. **(F)** TIRF images from reactions containing 1 μM of each actin isoform (10% Alexa-488 labeled α-actin (RMA)) and 1 nM mDia1(FH1-C). Scale bars, 10 μm. See also Movie 1. **(G)** Actin nucleation (n = 2-3 fields of view, represented as dots) counted from reactions as in **(F)** 100 s after the initiation of filament polymerization. ns, no significant differences detected.

(Figure 2A)(Hatano, et al., 2018). Under these conditions, α-, β-, or γ-actin each show similar levels of filament nucleation (Figure 2B). Actin filaments polymerizing in reactions containing β- or γ-actin elongated at similar rates of 11.1 subunits s^{-1} μM^{-1} ± 0.3 (SEM) or 12.7 subunits s^{-1} μM^{-1} ± 0.2, respectively (Figure 2C). The rates for γ-actin were statistically faster than α-actin (RMA; 10.0 subunits s^{-1} μM^{-1} ± 0.3; p = 0.0002), β-actin, and the 1:1 mixture of β- and γ-actin isoforms (10.9 ± 0.3 subunits s^{-1} μM^{-1}; p = 0.0003) (Figure 2C). Thus, both recombinant β- and γ-actin polymerize into filaments and can co-polymerize (Figure 2C).

Cellular actin functions are further modulated through interactions with many regulatory proteins. Thus, we assessed the activities of several classic regulators of actin dynamics in the presence of either β- or γ-actin. First, we tested whether the classic actin disassembly protein cofilin could bind either actin isoform in pelleting assays (Figure 3A-B). Depending on conditions, protein sources and pH, cofilin can bind to actin monomers (present in G-buffer) or filaments (present in F-buffer) and can have filament stabilizing or destabilizing effects. In either condition tested here and regardless of actin source or isoform, cofilin bound actin monomers (Figure 3A) or filaments (Figure 3B), consistent with its normal concentration-dependent functions (Bobkov et al., 2006; De La Cruz, 2005; De La Cruz and Sept, 2010).

Although absent in budding yeast, thymosin-β4 (Tβ4), sequesters actin monomers to ultimately regulate the pool of subunits available for filament polymerization in mammalian cells (Skruber et al., 2018; Skruber et al., 2020). We used fluorescence polarization to determine the binding affinities of GFP-Tβ4 for β-, γ-, or α-actin (Figure 3C). GFP-Tβ4 bound to each isoform of actin, binding β-actin (k_D = 1.1 ± 0.3 nM (SEM)) and γ-actin (k_D = 1.0 ± 0.1 nM) with similar affinities, which were significantly stronger than RMA (k_D = 7.7 nM ± 0.4; p < 0.002) (Figure 3C).

In addition to Tβ4, profilin binds actin monomers and directly inhibits actin assembly by sterically blocking the site of new filament growth (Ferron et al., 2007; Pimm et al., 2020; Skruber et al., 2018). In contrast, when present with other filament promoting factors like ENA/VASP or formins, profilin can stimulate actin polymerization at rates greater than actin alone (Chesarone et al., 2010; Li and Higgs, 2003; Valencia and Quinlan, 2021). Thus, we compared how β- or γ-actin interacts with human profilin. To assess the extent that profilin was able to block the assembly of β- or γ-actin filaments, we used filament pelleting assays at different stoichiometries of profilin and actin (Figure 3D-E). As expected, the total amount of actin filament mass was reduced in reactions with higher ratios of profilin:actin, indicating profilin blocked the assembly of either actin isoform (Figure 3D-E). To explore whether either actin isoform could be used by formin proteins to assemble actin filaments, we measured filament nucleation from TIRF movies containing 1 μM actin (β, γ, or α) and 1 nM of the constitutively active formin, mDia1(FH1-C). Compared to actin alone controls, formin-based actin filament nucleation was enhanced for each actin isoform tested (Figure 2A-B and Figure 3F-G). While most of the actin polymer produced by formin is made in the nucleation phase of fil-

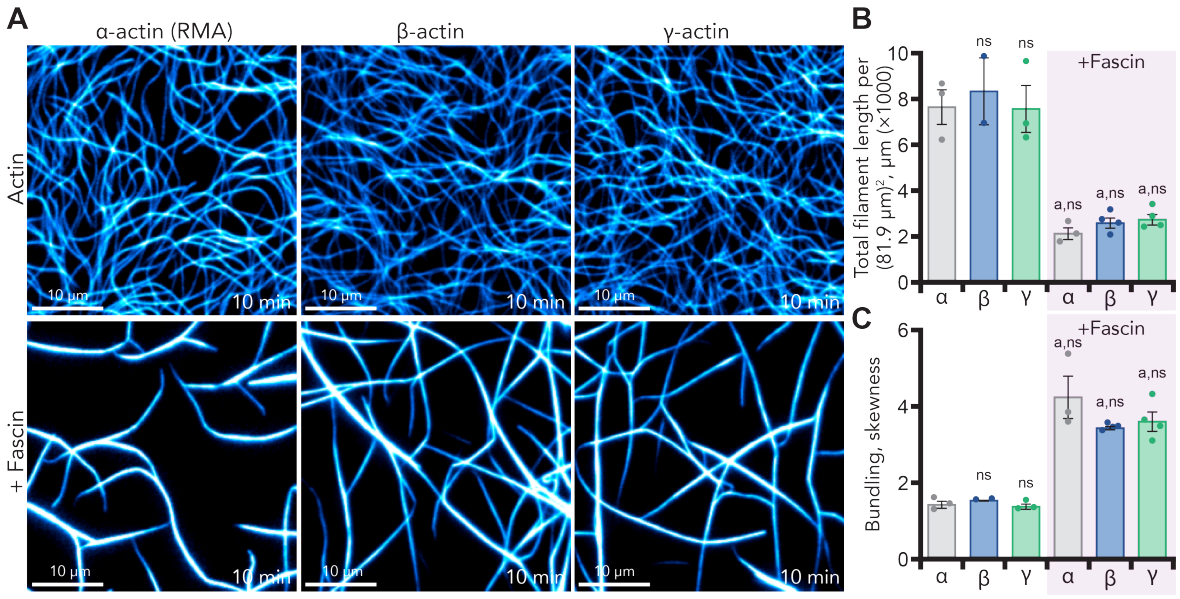

Figure 4. Fascin-mediated actin filament bundling of actin isoforms. (A) Representative TIRF images from reactions containing 1 µM of each unlabeled actin isoform and 130 nM Alexa-488 phalloidin, in the absence or presence of 1 µM fascin. Scale bars, 10 µm. **(B)** Ridge detection analysis of total filament polymer from reactions as in (A). **(C)** Extent of filament bundling (skewness) analysis from reactions as in (A). Analyses in (B) and (C) were performed 10 min after the initiation of filament polymerization and assessed per (81.9 µm)^2 field of view. Dots represent individual measurements. Error bars represent SEM. a, significantly different ($p<0.05$) than α-actin (RMA) without fascin. No significant difference was detected between individual isoforms for either analysis in (B) or (C) by one-way ANOVA with Tukey post-hoc analysis.

ament assembly (Courtemache, 2018; Zweifel et al., 2021), we also assessed whether the filament elongation was influenced by actin isoform in similar assays performed the presence of both profilin and mDia1(FH1-C). Indeed, actin assembly was further stimulated for either isoform as evident by the presence of longer actin filaments and enhanced total polymer mass in experiments including profilin and formin (Figure 2A-B, Figure 3F, Figure S3, and Movie 1). In sum, the nucleation of β- and γ-actin is suppressed by profilin (Figure 3D-E). In contrast, filament assembly (both nucleation and elongation) is enhanced by each actin isoform present as profilin-actin with formin (Figure 3F, Figure S3, and Movie 1).

Finally, the higher-order organization of cellular actin arrays is commonly achieved through the association of proteins that cross-link or bundle filaments. Thus, we chose the canonical actin bundling protein fascin to compare bundles of actin filaments generated by either actin isoform with RMA. We produced fascin-bundles with equal concentrations of fascin and unlabeled (pure) β-actin, γ-actin, or α-actin, and then visualized actin with Alexa-488 phalloidin and TIRF microscopy (Figure 4A). Regardless of actin isoform, reactions containing fascin produced bundled actin filaments. As actin filaments bundled the overall area covered by actin filament signal decreases. Meanwhile, the distribution of pixel intensities in an image shift toward brighter pixels intensities as the extent of filament bundling increases (Higaki et al., 2010; Khurana et al., 2010). Therefore, we quantitatively measured the extent of actin filament bundling in experiments containing fascin using length and fluorescence intensity-based metrics to assess filament bundling (Figure 4B-C). Ridge detection analysis measured the overall length of discreet linear objects, which decreased over time as actin filaments coalesced into bundles generated from β-, γ-, or α-actin (Figure 4B). In contrast, fluorescence intensity of actin filaments made by β-, γ-, and α-actin each became brighter as they were crosslinked by fascin (Figure 4C). In sum, β-, γ-, and α-actin are equally responsive to filament bundling by fascin.

Discussion

We developed budding yeast strains for the expression and purification of recombinant human cytoplasmic β- and γ-actin and have demonstrated that these actin isoforms polymerize and interact with several canonical actin binding proteins. There are several benefits to purifying recombinant actin from this system including: high yield (0.5-1 mg/L starting yeast culture), no special growth requirements, use of conventional purification reagents and protocols, no additional post-purification processing (e.g., cleavage of fusion tags), and no concern over removal of contaminating "host" actin. Even with these advantages, we note that for both yeast and human actin purifications, a significant amount of protein (>50%) is lost following post-elution dialysis. This may reflect the denaturing activity of the formamide used to elute actin from the DNaseI column and may be improved by supplementing our approach with an alternative 6×His-gelsolin fragment-based purification (Ohki et al., 2009).

Comparisons of actin isoforms or mixes that reflect other species and non-muscle cells are crucial to our understanding of how actin and its regulators truly function. For example, the formin FHOD1 displays differential interactions with actin from different sources, specifically enhancing the nucleation phase of actin assembly with cytoplasmic actin but preventing the assembly of filaments generated from rabbit muscle actin (Antoku et al., 2019; Patel et al., 2018). Profilin

and cofilin each bind cytoplasmic actin with higher affinity than muscle actin (Antoku et al., 2019; De La Cruz, 2005; Kinosian et al., 2000). Further, specific myosin motors differentially prefer muscle or non-muscle sources, some even preferring specific β- over γ-actin isoforms for movements (Muller et al., 2013). Our results further identify thymosin-β4 as an additional actin regulatory protein influenced by actin source, binding β- or γ-actin with higher affinity than actin purified from muscle.

A potential drawback of our system is that yeast-produced actin may lack specific post-translational processing important for an interaction or process of interest to the investigator. Over 100 post-translational modifications (PTMs) of actin have been described, including commonly reported acetylation, arginylation, methylation, and phosphorylation, and have each been described for multiple actin isoforms (Terman and Kashina, 2013; Varland et al., 2019). Most relevant for the discussion of either actin isoform are acetylation or arginylation as β- and γ-actin differ by only four residues at the N-terminus near these modified sites (Figure 1A). Most human actin is processed to remove the N-terminal methionine and then acetylated at the second or third residue or less commonly (and only for β-actin) arginylated at Asp3 (Varland et al., 2019). These PTMs may influence the rate of actin polymerization, filament-filament interactions, actin-binding protein interactions, cellular localization, and locomotion (Arnesen et al., 2018; Bergeron et al., 2010; Karakozova et al., 2006; Miller et al., 1996; Pavlyk et al., 2018; Saha et al., 2010; Varland et al., 2019; Yamashiro et al., 2014). Here we found the β-actin was processed removing the first two or three amino acids and arginylation was present at Asp3 for a subset of molecules. We did not find evidence of N-terminal acetylation on this β-actin. In contrast, γ-actin produced from budding yeast appears uniformly acetylated at the N-terminal methionine, similar to the reported processing of yeast actin (Cook et al., 1991). Although N-terminal differences may be important for some applications, they appear to be less consequential for others (Cook et al., 1992; Hatano et al., 2018). Thus, should the strict nature of PTMs at or near the N-terminus of actin become "mission critical", an alternative *Pichia*-based system may prove advantageous or a useful partner to our method (Hatano et al., 2020).

Supplemental information

Supplemental information associated with this work includes: one table, three figures, and one movie.

Acknowledgements

We thank Stephan Wilkens and Rebecca Oot (SUNY Upstate) for the use of their FPLC and Superdex 75 column and assistance with protein labeling, Tom Duncan, Stewart Loh, Leszek Kotula and the SUNY Upstate Department of Biochemistry and Molecular Biology for the use and maintenance of crucial equipment, Marcella Alcaide Eligio (Hunter College) for assistance with fascin purification, and Marc Ridilla for critically reading the manuscript. This work was supported by NIH grants R01 GM056189 to DCA, R35 GM133485 to JLH-R, the Research Foundation of SUNY, and SUNY Upstate Medical University.

Competing interests

The authors declare no competing interests.

Author contributions

DCA, BKH, and JLH-R conceived of the project; BKH, JHL-R, MP, and EPdJ performed the experiments; EdJ performed mass spectrometry and analyzed resulting data; all authors contributed to writing and editing the manuscript.

References

1. Aggeli, D., E. Kish-Trier, M.C. Lin, B. Haarer, G. Cingolani, J.A. Cooper, S. Wilkens, and D.C. Amberg. 2014. Coordination of the filament stabilizing versus destabilizing activities of cofilin through its secondary binding site on actin. *Cytoskeleton*. 71:361-379.

2. Allen, P.G., C.B. Shuster, J. Kas, C. Chaponnier, P.A. Janmey, and I.M. Herman. 1996. Phalloidin binding and rheological differences among actin isoforms. *Biochemistry*. 35:14062-14069.

3. Antoku, S., W. Wu, L.C. Joseph, J.P. Morrow, H.J. Worman, and G.G. Gundersen. 2019. ERK1/2 Phosphorylation of FHOD connects signaling and nuclear positioning alternations in cardiac laminopathy. *Developmental Cell*. 51:602-616 e612.

4. Arnesen, T., R. Marmorstein, and R. Dominguez. 2018. Actin's N-terminal acetyltransferase uncovered. *Cytoskeleton*. 75:318-322.

5. Belmont, L.D., A. Orlova, D.G. Drubin, and E.H. Egelman. 1999. A change in actin conformation associated with filament instability after Pi release. *Proceedings of the National Academy of Sciences of the United States of America*. 96:29-34.

6. Bergeron, S.E., M. Zhu, S.M. Thiem, K.H. Friderici, and P.A. Rubenstein. 2010. Ion-dependent polymerization differences between mammalian beta- and gamma-nonmuscle actin isoforms. *The Journal of Biological Chemistry*. 285:16087-16095.

7. Bobkov, A.A., A. Muhlrad, D.A. Pavlov, K. Kokabi, A. Yilmaz, and E. Reisler. 2006. Cooperative effects of cofilin (ADF) on actin structure suggest allosteric mechanism of cofilin function. *Journal of Molecular Biology.* 356:325-334.

8. Bookwalter, C.S., and K.M. Trybus. 2006. Functional consequences of a mutation in an expressed human alpha-cardiac actin at a site implicated in familial hypertrophic cardiomyopathy. *The Journal of Biological Chemistry*. 281:16777-16784.

9. Chesarone, M.A., A.G. DuPage, and B.L. Goode. 2010. Unleashing formins to remodel the actin and microtubule cytoskeletons. *Nature Reviews Molecular Cell Biology*. 11:62-74.

10. Clark, M.G., and D.C. Amberg. 2007. Biochemical and genetic analyses provide insight into the structural and mechanistic properties of actin filament disassembly by the Aip1p cofilin complex in S*accharomyces cerevisiae*. *Genetics*. 176:1527-1539.

11. Cook, R.K., W.T. Blake, and P.A. Rubenstein. 1992. Removal of the amino-terminal acidic residues of yeast actin. Studies *in vitro* and *in vivo*. *The Journal of Biological Chemistry*. 267:9430-9436.

12. Cook, R.K., D.R. Sheff, and P.A. Rubenstein. 1991. Unusual metabolism of the yeast actin amino terminus. *The Journal of Biological Chemistry*. 266:16825-16833.

13. Courtemanche, N. 2018. Mechanisms of formin-mediated actin assembly and dynamics. *Biophysical Reviews*. 10:1553-1569.

14. De La Cruz, E.M. 2005. Cofilin binding to muscle and non-muscle actin filaments: isoform-dependent cooperative interactions. *Journal of Molecular Biology*. 346:557-564.

15. De La Cruz, E.M., and D. Sept. 2010. The kinetics of cooperative cofilin binding reveals two states of the cofilin-actin filament. *Biophysical Journal*. 98:1893-1901.

16. Ferron, F., G. Rebowski, S.H. Lee, and R. Dominguez. 2007. Structural basis for the recruitment of profilin-actin complexes during filament elongation by Ena/VASP. *EMBO Journal*. 26:4597-4606.

17. Geissler, S., K. Siegers, and E. Schiebel. 1998. A novel protein complex promoting formation of functional alpha- and gamma-tubulin. *EMBO Journal*. 17:952-966.

18. Grantham, J. 2020. The molecular chaperone CCT/TRiC: an essential component of proteostasis and a potential modulator of protein aggregation. *Frontiers in Genetics*. 11:172.

19. Haarer, B.K., S.H. Lillie, A.E. Adams, V. Magdolen, W. Bandlow, and S.S. Brown. 1990. Purification of profilin from *Saccharomyces cerevisiae* and analysis of profilin-deficient cells. *The Journal of Cell Biology*. 110:105-114.

20. Hatano, T., S. Alioto, E. Roscioli, S. Palani, S.T. Clarke, A. Kamnev, J.R. Hernandez-Fernaud, L. Sivashanmugam, Y.L.B. Chapa, A.M.E. Jones, R.C. Robinson, K. Sampath, M. Mishima, A.D. McAinsh, B.L. Goode, and M.K. Balasubramanian. 2018. Rapid production of pure recombinant actin isoforms in *Pichia pastoris*. *Journal of Cell Science*. 131.

21. Hatano, T., L. Sivashanmugam, A. Suchenko, H. Hussain, and M.K. Balasubramanian. 2020. Pick-ya actin - a method to purify actin isoforms with bespoke key post-translational modifications. *Journal of Cell Science*. 133.

22. Henty-Ridilla, J.L. 2022. Visualizing actin and microtubule coupling dynamics in vitro by Total Internal Reflection Fluorescence (TIRF) microscopy. *The Journal of Visualized Experiments*. e64074.

23. Higaki, T., N. Kutsuna, T. Sano, N. Kondo, and S. Hasezawa. 2010. Quantification and cluster analysis of actin cytoskeletal structures in plant cells: role of actin bundling in stomatal movement during diurnal cycles in Arabidopsis guard cells. *The Plant Journal*. 61:156-165.

24. Hundt, N., M. Preller, O. Swolski, A.M. Ang, H.G. Mannherz, D.J. Manstein, and M. Muller. 2014. Molecular mechanisms of disease-related human beta-actin mutations p.R183W and p.E364K. *FEBS Journal*. 281:5279-5291.

25. Jansen, S., A. Collins, C. Yang, G. Rebowski, T. Svitkina, and R. Dominguez. 2011. Mechanism of actin filament bundling by fascin. *The Journal of Biological Chemistry*. 286:30087-30096.

26. Karakozova, M., M. Kozak, C.C. Wong, A.O. Bailey, J.R. Yates, 3rd, A. Mogilner, H. Zebroski, and A. Kashina. 2006. Arginylation of beta-actin regulates actin cytoskeleton and cell motility. *Science*. 313:192-196.

27. Karlsson, R. 1988. Expression of chicken beta-actin in *Saccharomyces cerevisiae*. *Gene*. 68:249-257.

28. Karlsson, R., P. Aspenstrom, and A.S. Bystrom. 1991. A chicken beta-actin gene can complement a disruption of the *Saccharomyces cerevisiae ACT1* gene. *Molecular and Cellular Biology*. 11:213-217.

29. Khurana, P., J.L. Henty, S. Huang, A.M. Staiger, L. Blanchoin, and C.J. Staiger. 2010. *Arabidopsis* VILLIN1 and VILLIN3 have overlapping and distinct activities in actin bundle formation and turnover. *The Plant Cell*. 22:2727-2748.

30. Kijima, S.T., K. Hirose, S.G. Kong, M. Wada, and T.Q. Uyeda. 2016. Distinct biochemical properties of *Arabidopsis thaliana* actin isoforms. *Plant and Cell Physiology*. 57:46-56.

31. Kinosian, H.J., L.A. Selden, L.C. Gershman, and J.E. Estes. 2000. Interdependence of profilin, cation, and nucleotide binding to vertebrate non-muscle actin. *Biochemistry*. 39:13176-13188.

32. Li, F., and H.N. Higgs. 2003. The mouse Formin mDia1 is a potent actin nucleation factor regulated by autoinhibition. *Current Biology*. 13:1335-1340.

33. Liu, X., M.L. Pimm, B. Haarer, A.T. Brawner, and J.L. Henty-Ridilla. 2022. Biochemical characterization of actin assembly mechanisms with ALS-associated profilin variants. *The European Journal of Cell Biology*. 101:151212.

34. Millan-Zambrano, G., and S. Chavez. 2014. Nuclear functions of prefoldin. *Open Biology*. 4.

35. Miller, C.J., W.W. Wong, E. Bobkova, P.A. Rubenstein, and E. Reisler. 1996. Mutational analysis of the role of the N terminus of actin in actomyosin interactions. Comparison with other mutant actins and implications for the cross-bridge cycle. *Biochemistry*. 35:16557-16565.

36. Moradi, M., R. Sivadasan, L. Saal, P. Luningschror, B. Dombert, R.J. Rathod, D.C. Dieterich, R. Blum, and M. Sendtner. 2017. Differential roles of alpha-, beta-, and gamma-actin in axon growth and collateral branch formation in motoneurons. *The Journal of Cell Biology*. 216:793-814.

37. Muller, M., R.P. Diensthuber, I. Chizhov, P. Claus, S.M. Heissler, M. Preller, M.H. Taft, and D.J. Manstein. 2013. Distinct functional interactions between actin isoforms and nonsarcomeric myosins. *PLoS ONE*. 8:e70636.

38. Muller, M., A.J. Mazur, E. Behrmann, R.P. Diensthuber, M.B. Radke, Z. Qu, C. Littwitz, S. Raunser, C.A. Schoenenberger, D.J. Manstein, and H.G. Mannherz. 2012. Functional characterization of the human alpha-cardiac actin mutations Y166C and M305L involved in hypertrophic cardiomyopathy. *Cellular and Molecular Life Sciences*. 69:3457-3479.

39. Namba, Y., M. Ito, Y. Zu, K. Shigesada, and K. Maruyama. 1992. Human T cell L-plastin bundles actin filaments in a calcium-dependent manner. *Journal of Biochemistry*. 112:503-507.

40. Noguchi, T.Q., N. Kanzaki, H. Ueno, K. Hirose, and T.Q. Uyeda. 2007. A novel system for expressing toxic actin mutants in Dictyostelium and purification and characterization of a dominant lethal yeast actin mutant. *The Journal of Biological Chemistry*. 282:27721-27727.

41. Ohki, T., C. Ohno, K. Oyama, S.V. Mikhailenko, and S. Ishiwata. 2009. Purification of cytoplasmic actin by affinity chromatography using the C-terminal half of gelsolin. *Biochemical and Biophysical Research Communications*. 383:146-150.

42. Patel, A.A., Z.A. Oztug Durer, A.P. van Loon, K.V. Bremer, and M.E. Quinlan. 2018. Drosophila and human FHOD family formin proteins nucleate actin filaments. *The Journal of Biological Chemistry.* 293:532-540.

43. Pavlyk, I., N.A. Leu, P. Vedula, S. Kurosaka, and A. Kashina. 2018. Rapid and dynamic arginylation of the leading edge beta-actin is required for cell migration. *Traffic*. 19:263-272.

44. Perrin, B.J., and J.M. Ervasti. 2010. The actin gene family: function follows isoform. *Cytoskeleton*. 67:630-634.

45. Pimm, M.L., J. Hotaling, and J.L. Henty-Ridilla. 2020. Profilin choreographs actin and microtubules in cells and cancer. *International Review of Cell and Molecular Biology*. 355:155-204.

46. Pimm, M.L., X. Liu, F. Tuli, J. Heritz, A. Lojko, and J.L. Henty-Ridilla. 2022. Visualizing molecules of functional human profilin. *eLife*. 11.

47. Rappsilber, J., Y. Ishihama, and M. Mann. 2003. Stop and go extraction tips for matrix-assisted laser desorption/ionization, nanoelectrospray, and LC/MS sample pretreatment in proteomics. *Analytical Chemistry*. 75:663-670.

48. Rutkevich, L.A., D.J. Teal, and J.F. Dawson. 2006. Expression of actin mutants to study their roles in cardiomyopathy. *Canadian Journal of Physiology Pharmacology*. 84:111-119.

49. Saha, S., M.M. Mundia, F. Zhang, R.W. Demers, F. Korobova, T. Svitkina, A.A. Perieteanu, J.F. Dawson, and A. Kashina. 2010. Arginylation regulates intracellular actin polymer level by modulating actin properties and binding of capping and severing proteins. *Molecular Biology of the Cell*. 21:1350-1361.

50. Schindelin, J., I. Arganda-Carreras, E. Frise, V. Kaynig, M. Longair, T. Pietzsch, S. Preibisch, C. Rueden, S. Saalfeld, B. Schmid, J.Y. Tinevez, D.J. White, V. Hartenstein, K. Eliceiri, P. Tomancak, and A. Cardona. 2012. Fiji: an open-source platform for biological-image analysis. *Nature Methods*. 9:676-682.

51. Sheffield, P., S. Garrard, and Z. Derewenda. 1999. Overcoming expression and purification problems of RhoGDI using a family of "parallel" expression vectors. *Protein Expression and Purification*. 15:34-39.

52. Shevchenko, A., H. Tomas, J. Havlis, J.V. Olsen, and M. Mann. 2006. In-gel digestion for mass spectrometric characterization of proteins and proteomes. *Nature Protocols*. 1:2856-2860.

53. Skruber, K., T.A. Read, and E.A. Vitriol. 2018. Reconsidering an active role for G-actin in cytoskeletal regulation. *Journal of Cell Science*. 131.

54. Skruber, K., P.V. Warp, R. Shklyarov, J.D. Thomas, M.S. Swanson, J.L. Henty-Ridilla, T.A. Read, and E.A. Vitriol. 2020. Arp2/3 and Mena/VASP require Profilin1 for actin network assembly at the leading edge. *Current Biology*. 30:2651-2664 e2655.

55. Steger, C. 1998. An unbiased detector of curvilinear structures. *IEEE Transactions on Pattern Analysis and Machine Intelligence*. 20:113-125.

56. Tamura, M., K. Ito, S. Kunihiro, C. Yamasaki, and M. Haragauchi. 2011. Production of human beta-actin and a mutant using a bacterial expression system with a cold shock vector. *Protein Expression and Purification*. 78:1-5.

57. Terman, J.R., and A. Kashina. 2013. Post-translational modification and regulation of actin. *Current Opinion in Cell Biology*. 25:30-38.

58. Valencia, D.A., and M.E. Quinlan. 2021. Formins. *Current Biology*. 31:R517-R522.

59. Valpuesta, J.M., J. Martin-Benito, P. Gomez-Puertas, J.L. Carrascosa, and K.R. Willison. 2002. Structure and function of a protein folding machine: the eukaryotic cytosolic chaperonin CCT. *FEBS Letters*. 529:11-16.

60. Varland, S., J. Vandekerckhove, and A. Drazic. 2019. Actin post-translational modifications: the Cinderella of cytoskeletal control. *Trends in Biochemical Sciences*. 44:502-516.

61. von der Ecken, J., S.M. Heissler, S. Pathan-Chhatbar, D.J. Manstein, and S. Raunser. 2016. Cryo-EM structure of a human cytoplasmic actomyosin complex at near-atomic resolution. *Nature*. 534:724-728.

62. Wagner, T., M. Hiner, and Xraynaud. 2017. Thorstenwagner/Ij-Ridgedetection: Ridge detection 1.4.0. Zenodo.

63. Wang, F., R.V. Sampogna, and B.R. Ware. 1989. pH dependence of actin self-assembly. *Biophysical Journal*. 55:293-298.

64. Wen, K.K., X. Yao, and P.A. Rubenstein. 2002. GTP-yeast actin. *The Journal of Biological Chemistry*. 277:41101-41109.

65. Yamashiro, S., D.S. Gokhin, Z. Sui, S.E. Bergeron, P.A. Rubenstein, and V.M. Fowler. 2014. Differential actin-regulatory activities of Tropomodulin1 and Tropomodulin3 with diverse tropomyosin and actin isoforms. *The Journal of Biological Chemistry*. 289:11616-11629.

66. Zweifel, M.E., L.A., Sherer, B. Mahanta, and N. Courtemanche. 2021 Nucleation limits the lengths of actin filaments assembled by formin. *Biophysical Journal*. 120:4442-4456.

Supplemental Information

Table 1. Oligonucleotide primers used in this study.

Primer Name	Sequence	Gene/Feature	Purpose
ACTB-G1	CTCGGATCCATGGAAGAAGAAATTGCTGC ATTGGTTATTGATAATGGTTCTGGCATGTG	ACTB/ACTG1	PCR/change optimized ACTB to ACTG1
GPD-RI	GTGAGAATTCTCAGTTCGAGTTTATCATTA	TDH3/GPD promoter	PCR 681 bp GPD promoter
GPD-Bam	CTCGGATCCTTTGTTTGTTTATGTGTGTTT	TDH3/GPD promoter	PCR 681 bp GPD promoter
HsPFN1-F	GTGAGAATTCATGGCCGGGTGGAACGCC	Hs profilin-1	Cloning into pKK223
HsPFN1-R	GTGAAAGCTTTCAGTACTGGGAACGCCG	Hs profilin-1	Cloning into pKK223
HsCFL1-3	GGCGCCATGGCCTCCGGTGTGGCTGTCTCTG	Hs-cofilin-1	Cloning into pGST-Parallel
HsCFL1-2	GTGAGAATTCTCACAAAGGCTTGCCCTCC	Hs-cofilin-1	Cloning into pGST-Parallel

Supplemental Figures and Legends

A

ACTB (β-actin):

ggatccATGGATGATGATATTGCTGCATTGGTTGTTGATAATGGTTCTGGCATGTGTAAAGC
TGGTTTTGCAGGTGACGATGCTCCAAGAGCAGTTTTTCCATCAATTGTTGGTAGACCAA
GACATCAAGGTGTTATGGTTGGTATGGGTCAAAAAGATTCTTATGTTGGTGACGAAGCTC
AATCAAAGAGAGGTATTTTGACATTGAAGTACCCAATCGAACATGGTATCGTTACTAACTG
GGATGATATGGAAAAGATTTGGCATCATACATTCTACAACGAATTGAGAGTTGCTCCAGA
AGAACATCCAGTTTTGTTAACAGAAGCTCCATTAAACCCAAAGGCAAACAGAGAAAAGAT
GACTCAAATCATGTTCGAAACTTTTAATACTCCAGCTATGTACGTTGCTATTCAAGCAGTT
TTGTCTTTATACGCATCAGGTAGAACTACAGGTATTGTTATGGATTCTGGTGACGGTGTTA
CACATACTGTTCCAATCTATGAAGGTTACGCTTTGCCACATGCAATTTTGAGATTAGATTT
GGCTGGTAGAGATTTGACAGATTATTTGATGAAGATCTTGACTGAAAGAGGTTACTCTTT
TACTACAACTGCAGAAAGAGAAATCGTTAGAGATATCAAGGAAAAATTGTGTTACGTTGC
TTTGGATTTCGAACAAGAAATGGCAACAGCTGCATCTTCATCTTCATTGGAAAAATCATA
CGAATTACCAGATGGTCAAGTTATTACTATCGGTAACGAAAGATTCAGATGTCCAGAAGC
ATTGTTTCAACCATCATTTTTGGGTATGGAATCATGTGGTATTCATGAAACAACTTTTAATT
CTATCATGAAATGTGATGTTGATATTAGAAAAGATTTGTATGCTAATACAGTTTTATCAGGT
GGTACAACTATGTACCCAGGTATCGCAGATAGAATGCAAAAGGAAATCACAGCTTTGGCA
CCATCTACTATGAAGATTAAAATCATCGCTCCACCAGAAAGAAAGTATTCTGTTTGGATTG
GTGGTTCAATCTTGGCATCTTTGTCAACTTTCCAACAAATGTGGATCTCAAAGCAAGAAT
ACGATGAATCTGGTCCATCAATTGTTCATAGAAAATGTTTTtagcccgggaagct

B

ACTA1 (α1-actin):

ggatccATGTGTGATGAAGATGAAACTACAGCTTTAGTTTGTGATAATGGTTCTGGTTTGGT
TAAAGCTGGTTTTGCAGGTGACGATGCTCCAAGAGCAGTTTTTCCATCAATTGTTGGTA
GACCAAGACATCAAGGTGTTATGGTTGGTATGGGTCAAAAAGATTCTTATGTTGGTGACG
AAGCTCAATCAAAGAGAGGTATTTTGACTTTGAAGTACCCAATCGAACATGGTATCATCA
CAAACTGGGATGATATGGAAAAGATTTGGCATCATACTTTCTACAACGAATTGAGAGTTG
CACCAGAAGAACATCCAACTTTGTTAACAGAAGCTCCATTGAACCCAAAGGCAAACAGA
GAAAAGATGACTCAAATCATGTTCGAAACTTTTAATGTTCCAGCTATGTACGTTGCTATTC
AAGCAGTTTTGTCTTTATACGCATCAGGTAGAACTACAGGTATTGTTTTAGATTCTGGTGA
CGGTGTTACTCATAATGTTCCAATCTATGAAGGTTACGCTTTGCCACATGCAATTATGAGA
TTGGATTTGGCTGGTAGAGATTTGACTGATTATTTGATGAAGATCTTGACAGAAAGAGGT
TACTCTTTCGTTACTACAGCAGAAAGAGAAATCGTTAGAGATATCAAGGAAAAATTGTGTT
ACGTTGCTTTGGATTTCGAAAACGAAATGGCAACAGCTGCATCTTCATCTTCATTAGAAA
AATCATACGAATTGCCAGATGGTCAAGTTATTACTATCGGTAACGAAAGATTCAGATGTCC
AGAAACATTGTTCCAACCATCTTTTATTGGTATGGAATCAGCTGGTATTCATGAAACTACA
TACAACTCTATCATGAAGTGTGATATCGATATCAGAAAAGATTTGTATGCTAATAATGTTAT
GTCAGGTGGTACTACAATGTACCCAGGTATCGCAGATAGAATGCAAAAGGAAATCACTG
CTTTGGCACCATCTACAATGAAGATTAAAATCATCGCTCCACCAGAAAGAAAGTATTCTG
TTTGGATTGGTGGTTCAATCTTGGCATCTTTATCAACTTTCCAACAAATGTGGATCACAAA
GCAAGAATACGATGAAGCTGGTCCATCAATTGTTCATAGAAAATGTTTTtaacccgggaagctt

Figure S1. Sequences of yeast-optimized human recombinant actin isoforms. Codon-optimized coding sequences for **(A)** β-actin (ACTB) and **(B)** α1-actin (ACTA1) are indicated in upper case letters, whereas flanking sequences including engineered restriction sites are in lower case text.

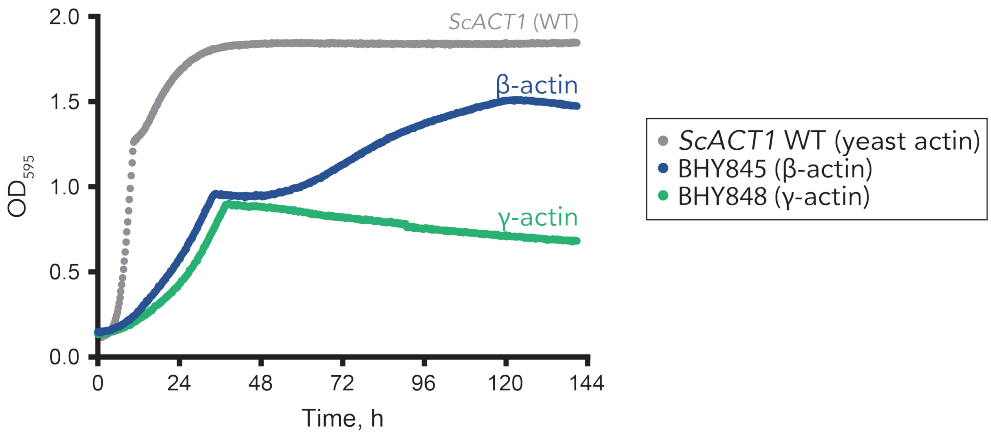

Figure S2. Growth of yeast expressing β- or γ-actin isoforms. Growth of actin isoform expressing yeast strains performed at 30 °C in YPD media.

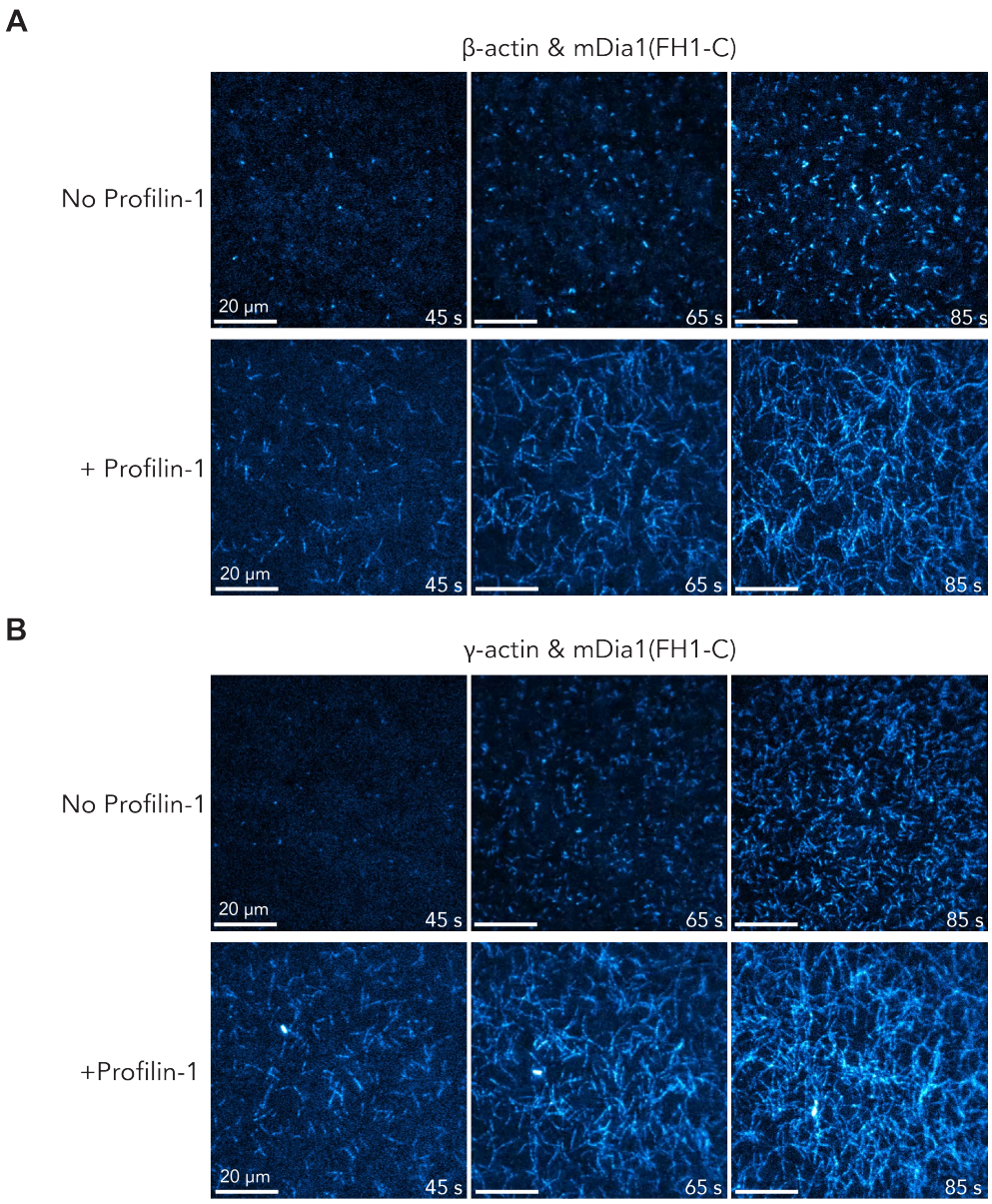

Figure S3. Formin and profilin stimulate actin filament elongation of with β- or γ-actin isoforms. **(A)** Images from time-lapse TIRF microscopy reactions containing 1 μM β-actin (10% Alexa-488 labeled α-actin (RMA)), 1 nM mDia1(FH1-C) (formin), and the absence (top) or presence (bottom) of 1 μM profilin-1. **(B)** Images as in (A) from reactions containing 1 μM γ-actin (10% Alexa-488 labeled α-actin (RMA)), 1 nM mDia1(FH1-C) (formin), and the absence (top) or presence (bottom) of 1 μM profilin-1. Scale bars, 20 μm. See also Movie 1. The presence of longer actin filaments and more abundant polymer mass strongly suggest the combination of profilin:β-actin or profilin:γ-actin support accelerated formin-based filament elongation.

Movie Legend

Movie 1. β- and γ-actin isoforms can be used by profilin and formin to nucleate and rapidly elongate actin filaments. TIRF microscopy images of reactions containing: 1 µM β- or γ-actin (10% Alexa-488 labeled α-actin (RMA)), 1 nM mDia1(FH1-C) (formin), and the absence (top) or presence (bottom) of 1 µM profilin-1. Scale bar, 20 µm. Playback, 10 fps.